Nonlinear Control of a Buck Converter Which Feeds a Constant Power Load

Jorge A. Solsona, *Senior Member, IEEE*, Sebastián Gómez Jorge, and Claudio A. Busada

***Abstract*—In this paper, a nonlinear control strategy for controlling a dc/dc buck converter feeding a constant power load is proposed. The main objective of the proposed controller is to improve the transient performance when in presence of unknown power disturbances. A feedback controller is combined with a feedforward strategy. A nonlinear reduced order observer is used for estimating the value of the power load and its time derivative. These estimated values are fed forward to the nonlinear feedback controller whose design is based on feedback linearization method. The proposed controller is tested via simulation and experimental results.**

***Index Terms*—Constant power load, dc/dc converters, feedforward compensation, power converters.**

I. Introduction

NOWADAYS, we are witnessing a paradigm shift in regard to the ways in which electrical energy is consumed. While the twentieth century was dominated by the design of generation systems with transmission and distribution of alternating current, preferably with large power plants far from the centers of consumption and with long transmission lines, it is clear that in the last two decades distributed generation has gained significant importance. This begins to form an important part of the energy generated for consumption in different places. This "new" model continuously receives incentives in industrialized countries, and there are new technologies being developed in order to improve it [1].

The dominant model of transmission and distribution was to use an ac voltage with sine wave, where transformers were used to change the voltage levels. However, in the new distribution scenario, it is not only necessary to modify the voltage levels but also its waveform. In addition, some of the emerging technologies for the generation, such as photovoltaic cells and fuel cells, are dc voltage generators. This leads to the proliferation of electronic voltage converters that perform the function of conversion (see [2] and references therein). Also, the way in which vehicles used for transport are powered is changing, mainly due to the advent of electric vehicles [3], [4]. Many times dc voltage is used in servomechanisms [5] and in communication applications [6].

It is for the above reasons, that there was a notorious increase in the amount of dc/dc voltage converters that are used in different applications. Moreover, new technologies are being applied to implement buck converters [7]. Generally, designers use control techniques for obtaining converters with high performance. Among others, a complete digital controller, a robust output feedback controller, a self-adaptive discontinuous conduction mode controller, and minimum time controller were presented in [8]–[11], respectively.

In several of these applications, converters transfer power to constant power loads. This happens, for example, in transport applications [12]–[14], in integration systems of wind and solar generators [15], [16], in building nanogrids and data centers [17], and in dc power distribution systems [18].

When converters feed constant power loads, a characteristic of negative resistance which complicates the situation, from a control viewpoint, is presented. The converters are inherently nonlinear systems, but it could be said, roughly speaking, that a constant power load increases the degree of nonlinearity [19].

In recent years, various researchers have focused on dealing with this problem and have proposed various control techniques in order to achieve high performance in systems that include dc/dc converters feeding constant power loads. It is possible to find in the literature, different strategies for stabilizing the system, such as the passive damping [20], pseudolinearization [21], interconnection with damping allocation [22], sliding-mode control [23], [24], fuzzy control with gain-scheduling [25], active damping [26], and flatness [27].

However, in this type of applications, it is possible to improve the performance of the system, regarding load disturbances, through a feedforward compensation that includes in the command signal information from the changes that occur in the load. This has been done, for example, using the measurement of the load current [28], but in this case, it is necessary to have an additional sensor on the control scheme.

One way to avoid the measurement of the load current is to replace it by an estimate obtained from other measured variables. This estimate can be computed efficiently through the use of observers [29], [30].

This paper proposes a strategy to control dc/dc converters that feed constant power loads. The law is obtained from feedback linearization, where the nonlinear transformation is a function of the power of an unknown load and its time derivative. Therefore, a nonlinear reduced order observer is used to estimate them, allowing their use for feedforward compensation in the control law. This compensation improves, from the disturbance rejection point of view, the performance compared to strategies that use only feedback controllers (see for instance [31]). The main feature of the proposal is, therefore, that it improves the transient response of the converter when in presence of a load disturbance. It is achieved by using a cheaper

Manuscript received April 10, 2014; revised June 18, 2014, August 29, 2014, and November 11, 2014; accepted January 3, 2015. Date of publication January 15, 2015; date of current version August 21, 2015. This work was supported by Universidad Nacional del Sur, CONICET and ANPCyT, Argentina. Recommended for publication by Associate Editor M. Ordonez.

All authors are with the Departamento de Ingeniería Eléctrica y de Computadoras, Instituto de Investigaciones en Ingeniería Eléctrica "Alfredo Desages", Universidad Nacional del Sur, 8000 Bahía Blanca, Argentina (e-mail: jsolsona@uns.edu.ar; sebastian.gomezjorge@uns.edu.ar; cbusada@uns.edu.ar).

Digital Object Identifier 10.1109/TPEL.2015.2392371

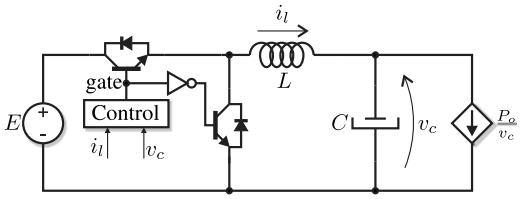

Fig. 1. Scheme of the system to be controlled.

and rugged controller, where the disturbance sensor has been avoided.

The rest of this paper is organized as follows: In Section II, the control system is described; in Section III, the proposed controller is presented, assuming that the load power is known. Then, in Section IV, the system behavior in presence of parametric uncertainties is analyzed. In Sections V and VI, simulation and experimental results are presented, respectively. Finally, in Section VII, conclusions are drawn.

II. System Description

Fig. 1 shows the scheme of the system to be controlled. This is composed of a buck converter and a controller, represented by the block "Control." The converter feeds a P_o constant power load, represented in the figure by a controlled current source. The controller requires the measurements of the voltage v_c and the current i_l. It will be assumed that the input voltage source E has a low impedance, and therefore, it is not disturbed by the load demand. It will also be assumed for the development of the control strategy that the converter is operating in continuous-conduction mode (CCM).

The averaged state model of the buck converter, in CCM , is [14]

$$L\dot{i}_l = Ed - v_c \tag{1}$$

$$C\dot{v}_c = i_l - \frac{P_o}{v_c} \tag{2}$$

where d is the converter duty cycle.

III. Proposed Controller

A. Nonlinear Control Law

The control of the converter is implemented through feedback linearization [32, pp. 545–569] . For this, the following change of variables is defined:

$$z_1 = \frac{1}{2}Cv_c^2 \tag{3}$$

$$z_2 = i_l v_c - P_o. \tag{4}$$

Differentiating these variables with respect to the time and using (1) and (2), the model of the converter in the new variables is described by

$$\begin{bmatrix}\dot{z}_1\\ \dot{z}_2\end{bmatrix} = \underbrace{\begin{bmatrix}0 & 1\\ 0 & 0\end{bmatrix}}_{A}\underbrace{\begin{bmatrix}z_1\\ z_2\end{bmatrix}}_{\vec{z}} + \underbrace{\begin{bmatrix}0\\ 1\end{bmatrix}}_{B} w \tag{5}$$

where

$$w = \frac{1}{L}\left[Ev_c d + \frac{L}{C}\left(i_l^2 - \frac{i_l}{v_c}P_o\right) - v_c^2\right] - m \tag{6}$$

and $m = \dot{P}_o$, the time derivative of P_o. As shown by (1) and (2), the plant state variable description is nonlinear. The change of variables in (3) and (4) is necessary in order to obtain a set of linear differential equations that group all the nonlinear terms in a single variable. This can be seen in (5), where w groups all the nonlinear terms.

Equation (6) suggests to choose the duty cycle as

$$d = \frac{1}{Ev_c}\left[L(w+m) + \frac{L}{C}\left(\frac{i_l}{v_c}P_o - i_l^2\right) + v_c^2\right]. \tag{7}$$

However, the actual values of the parameters (L and C) are unknown, and may differ from those loaded in the controller. Therefore, the duty cycle will be computed as

$$d = \frac{1}{Ev_c}\left[\hat{L}(d_1 + \hat{m}) + \frac{\hat{L}}{\hat{C}}\left(\frac{i_l}{v_c}\hat{P}_o - i_l^2\right) + v_c^2\right]. \tag{8}$$

In this equation, d_1 is the input of the linearized system. Parameters $\hat{L}$ and $\hat{C}$ are the assumed values of L and C, respectively, which are loaded to the controller. The signals $\hat{P}_o$ and $\hat{m}$ are the estimated values of P_o and m, respectively. In order to obtain an exact linearization, the assumed values of the parameters and signals involved in (8) must match their actual values. For the time being, it will be assumed that $\hat{L} = L$, $\hat{C} = C$, $\hat{P}_o = P_o$, and $\hat{m} = m$. Note that with these assumptions, using (8) yields a linear system (the effect of parameter mistuning will be analyzed later).

The variables built inside the controller using these parameters will be identified with tilde; therefore, (3) and (4) will be computed as

$$\tilde{z}_1 = \frac{1}{2}\hat{C}v_c^2 \tag{9}$$

$$\tilde{z}_2 = i_l v_c - \hat{P}_o. \tag{10}$$

With the above assumptions, $\tilde{z}_1 = z_1$ and $\tilde{z}_2 = z_2$, and therefore, d_1 coincides with w.

Note that the nonlinear transformation (10) includes the disturbance $\hat{P}_o$. Consequently, the controller (8) results in a combination of a feedback control law and a feedforward compensation.

Applying (8) in (5) and (6), the linearized model of the converter results

$$\dot{\vec{z}} = A\vec{z} + Bd_1. \tag{11}$$

Now linear control strategies can be applied. In this paper, the control is implemented through full-state feedback, as shown in Fig. 2. In this figure, the signal $\tilde{z}_1^*$ is the control reference, which is built through

$$\tilde{z}_1^* = \frac{1}{2}\hat{C}{v_c^*}^2 \tag{12}$$

where v_c^* is the desired reference voltage in the capacitor. To improve the performance in presence of parametric uncertainties, an integrator was added to the controller, represented by

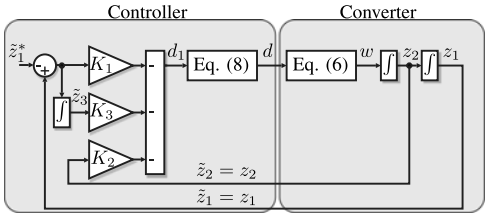

Fig. 2. Full state feedback of the linearized converter, assuming no parameter mismatch.

the state $\tilde{z}_3$. This allows to achieve zero steady-state error to a dc reference under parametric mismatches. With this additional state, from (5) and Fig. 2, the open-loop system is described by

$$\begin{bmatrix} \dot{z}_1 \\ \dot{z}_2 \\ \dot{\tilde{z}}_3 \end{bmatrix} = \underbrace{\begin{bmatrix} 0 & 1 & 0 \\ 0 & 0 & 0 \\ 1 & 0 & 0 \end{bmatrix}}_{A_1} \begin{bmatrix} z_1 \\ z_2 \\ \tilde{z}_3 \end{bmatrix} + \underbrace{\begin{bmatrix} 0 \\ 1 \\ 0 \end{bmatrix}}_{B_1} d_1 - \underbrace{\begin{bmatrix} 0 \\ 0 \\ 1 \end{bmatrix}}_{B_2} \tilde{z}_1^*. \quad (13)$$

B. Controller Gain Choice

According to Fig. 2, the feedback is given by

$$d_1 = -\underbrace{[K_1 \; K_2 \; K_3]}_{K} \begin{bmatrix} \tilde{z}_1 - \tilde{z}_1^* \\ \tilde{z}_2 \\ \tilde{z}_3 \end{bmatrix}. \quad (14)$$

Replacing (14) into (13), the closed-loop dynamics of the system is determined by the eigenvalues of

$$A_{cl} = A_1 - B_1 K = \begin{bmatrix} 0 & 1 & 0 \\ -K_1 & -K_2 & -K_3 \\ 1 & 0 & 0 \end{bmatrix} \quad (15)$$

that are obtained from the roots of the polynomial

$$\det(A_{cl} - \lambda I) = -(\lambda^3 + K_2\lambda^2 + K_1\lambda + K_3) \quad (16)$$

where I is the 3×3 identity matrix. To choose the gains, classical control theory will be used [33]. For this, a pair of dominant conjugate complex poles is chosen and the remaining real pole is made equal to ten times the real part of the dominant poles. For the second order system resulting from the dominant poles, the damping ζ, the natural resonance frequency ω_n, and the approximate settling time to 2% of the final value $t_{\rm set}$ are related as follows:

$$t_{\rm set} = \frac{3.91}{\zeta\omega_n}. \quad (17)$$

Choosing ζ and $t_{\rm set}$, the closed-loop poles will be

$$p_{1,2} = \omega_n(-\zeta \pm j\sqrt{1-\zeta^2}) \quad (18)$$

$$p_3 = -10\omega_n\zeta. \quad (19)$$

Then, the gain vector K of the controller can be found using A_{cl} and B_1 through Ackerman's method.

C. Load Power Estimation

The controller described in the previous section requires knowledge of the estimated value of the load power ($\hat{P}_o$) and the estimated value of its time derivative ($\hat{m}$) in order to compute (8). In this section, a reduced order observer will be used to estimate these variables. In order to build the observer, it will be assumed that the load power can be modeled as

$$\dot{P}_o = m \quad (20)$$

$$\dot{m} = 0. \quad (21)$$

The load model describes a load changing between different power values that are constant. The transient variation and the steady-state value are described by (20) and (21). During transients $m \neq 0$, while in steady state $m = 0$. With this assumption, the following observer is proposed:

$$\dot{\hat{z}}_1 = v_c i_l - \hat{P}_o \quad (22)$$

$$\dot{\hat{P}}_o = \hat{m} - g_1(\dot{\tilde{z}}_1 - \dot{\hat{z}}_1) \quad (23)$$

$$\dot{\hat{m}} = -g_2(\dot{\tilde{z}}_1 - \dot{\hat{z}}_1) \quad (24)$$

where g_1 and g_2 are gains to be defined. This observer requires the derivative of $\tilde{z}_1$; however, through a proper change of variables, this derivative will be avoided later.

D. Observer Gain Choice

Differentiating (9) with respect to time, note that $\dot{\tilde{z}}_1 - \dot{\hat{z}}_1 = \hat{P}_o - P_o$. Therefore, subtracting (23) from (20) and (24) from (21), the dynamics of the estimation errors of this observer are given by

$$\begin{bmatrix} \dot{e}_p \\ \dot{e}_m \end{bmatrix} = \underbrace{\begin{bmatrix} -g_1 & 1 \\ -g_2 & 0 \end{bmatrix}}_{\Phi} \begin{bmatrix} e_p \\ e_m \end{bmatrix} \quad (25)$$

where $e_p = P_o - \hat{P}_o$ and $e_m = m - \hat{m}$. The dynamics of the error is determined by the eigenvalues of the matrix Φ, which are obtained from the roots of the polynomial

$$\det(\Phi - \lambda I) = \lambda^2 + g_1\lambda + g_2. \quad (26)$$

Applying classical control theory again, the damping ζ_o, the natural resonance frequency ω_{no}, and the approximate settling time to 2% of the final value $t_{\rm seto}$ are related through:

$$g_1 = 2\zeta_o\omega_{no} \quad (27)$$

$$g_2 = \omega_{no}^2 \quad (28)$$

$$t_{\rm seto} = \frac{3.91}{\zeta_o\omega_{no}}. \quad (29)$$

Then, choosing ζ_o and $t_{\rm seto}$, the gains of the observer can be found. Note that in order to achieve a decoupling of the dynamics of the controller and the observer, it is recommended that $t_{\rm seto}$ is smaller than $t_{\rm set}$.

E. Observer Implementation

The implementation of the observer (22)–(24) requires knowledge of the time derivative of $\tilde{z}_1$. To avoid the computation of this derivative, the following change of variables is proposed:

$$\dot{\varepsilon}_1 = \dot{\hat{P}}_o + g_1\dot{\tilde{z}}_1 = \hat{m} + g_1\dot{\tilde{z}}_1 = \hat{m} + g_1(v_c i_l - \hat{P}_o) \quad (30)$$

$$\dot{\varepsilon}_2 = \dot{\hat{m}} + g_2\dot{\tilde{z}}_1 = g_2\dot{\tilde{z}}_1 = g_2(v_c i_l - \hat{P}_o) \quad (31)$$

where the terms of (23) and (24) with $\dot{z}_1$ were moved to the left, and (22) was replaced in the resulting equations. Integrating the second terms of these equations and solving it results

$$\hat{P}_o = \varepsilon_1 - g_1\tilde{z}_1 \quad (32)$$

$$\hat{m} = \varepsilon_2 - g_2\tilde{z}_1. \quad (33)$$

Then, replacing (32) and (33) into (30) and (31), the proposed observer can be computed through

$$\dot{\varepsilon}_1 = \varepsilon_2 - g_2\tilde{z}_1 + g_1(v_c i_l - \varepsilon_1 + g_1\tilde{z}_1) \quad (34)$$

$$\dot{\varepsilon}_2 = g_2(v_c i_l - \varepsilon_1 + g_1\tilde{z}_1). \quad (35)$$

The signals of interest, $\hat{P}_o$ and $\hat{m}$, are then recovered through (32) and (33).

F. Control Algorithm Summary

The complete control algorithm is summarized below

1) From the measured signals, $\tilde{z}_1$ is built through (9).
2) The differential equations (34), (35) are solved, and $\hat{P}_o$ and $\hat{m}$ are computed through (32), (33).
3) $\tilde{z}_2$ is computed through (10).
4) $\tilde{z}_1^*$ is computed through (12).
5) d_1 is computed through (14).
6) The duty cycle d is computed through (8).

IV. Behavior in Presence of Parameter Uncertainties

A. Observer Behavior

Let $\hat{C} = C - \triangle C$, where $\triangle C$ is a deviation of the capacitor value from its nominal value. Then, using this and (3), (9) can be rewritten as

$$\tilde{z}_1 = \frac{1}{2}(C - \triangle C)v_c^2 = z_1 - \frac{1}{2}\triangle C v_c^2. \quad (36)$$

Replacing (36) into (23) and (24), it results

$$\dot{\hat{P}}_o = \hat{m} - g_1(\dot{z}_1 - 2\triangle C v_c\dot{v}_c - \dot{\tilde{z}}_1) \quad (37)$$

$$\dot{\hat{m}} = -g_2(\dot{z}_1 - 2\triangle C v_c\dot{v}_c - \dot{\tilde{z}}_1). \quad (38)$$

The derivative of the error signals $e_p = P_o - \hat{P}_o$ and $e_m = m - \hat{m}$ now result

$$\dot{e}_p = e_m + g_1(\dot{z}_1 - \dot{\tilde{z}}_1) + g_1\triangle y \quad (39)$$

$$\dot{e}_m = g_2(\dot{z}_1 - \dot{\tilde{z}}_1) + g_2\triangle y \quad (40)$$

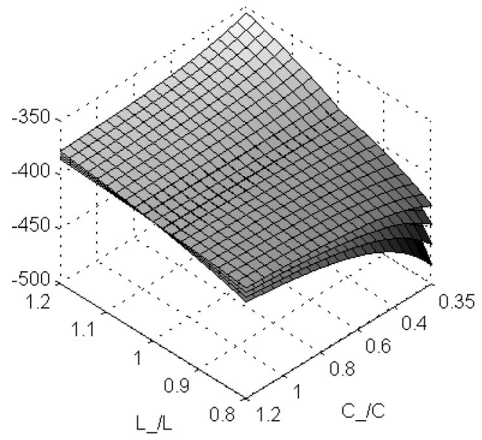

Fig. 3. Maximum real part of the closed-loop poles of the linearized system to a ±20% variation in $\hat{L}$ and $\hat{C}$. Each surface depicts output power increments of 125 W, from $P_o = 0$ to 500 W.

where $\triangle y = -2\triangle C v_c\dot{v}_c = -\frac{2\triangle C}{C}(i_l \;\; v_c - P_o)$. These last equations can be written in matrix form as follows:

$$\begin{bmatrix}\dot{e}_p\\ \dot{e}_m\end{bmatrix} = \underbrace{\begin{bmatrix}-g_1 & 1\\ -g_2 & 0\end{bmatrix}}_{\Phi}\underbrace{\begin{bmatrix}e_p\\ e_m\end{bmatrix}}_{e} + \underbrace{\begin{bmatrix}g_1\\ g_2\end{bmatrix}}_{g}\triangle y \quad (41)$$

or written more compactly

$$\dot{e} = \Phi e + g\triangle y. \quad (42)$$

Defining the Lyapunov candidate function $V = e^T e$, its derivative results

$$\begin{aligned}\dot{V} &= \dot{e}^T\, e + e^T\,\dot{e} = (e^T\,\Phi^T + \triangle y\, g^T)e + e^T(\Phi\, e + g\,\triangle y)\\ &= e^T(\Phi^T + \Phi)e + 2\triangle y\, g^T e \le -q\, e^T\, e\\ &\quad + 2||g||\,||e||\,||\triangle y|| \end{aligned} \quad (43)$$

where q is the minimum eigenvalue of Q, a positive definite matrix, solution of $\Phi^T + \Phi = -Q$. Then,

$$\begin{aligned}\dot{V} &\le -q||e||^2 + 2||g||\,||e||\,||\triangle y||\\ &\le -q\,V + 2||g||\sqrt{V}||\triangle y||. \end{aligned} \quad (44)$$

Now, dividing both sides of the inequation by $2\sqrt{V} > 0$, it results

$$\frac{\dot{V}}{2\sqrt{V}} \le -\underbrace{\frac{q}{2}}_{\gamma_1}\sqrt{V} + \underbrace{||g||\,||\triangle y||}_{\gamma_2} \le -\gamma_1\sqrt{V} + \gamma_2. \quad (45)$$

If $\rho = \sqrt{V}$, the inequation results

$$\dot{\rho} \le -\gamma_1\rho + \gamma_2. \quad (46)$$

This inequation can be solved using the comparison lemma ([32], p. 85)

$$\rho(t) \le exp^{-\gamma_1 t}\rho(0) + \int_0^t exp^{-\gamma_1(t-\tau)}\gamma_2 d\tau. \quad (47)$$

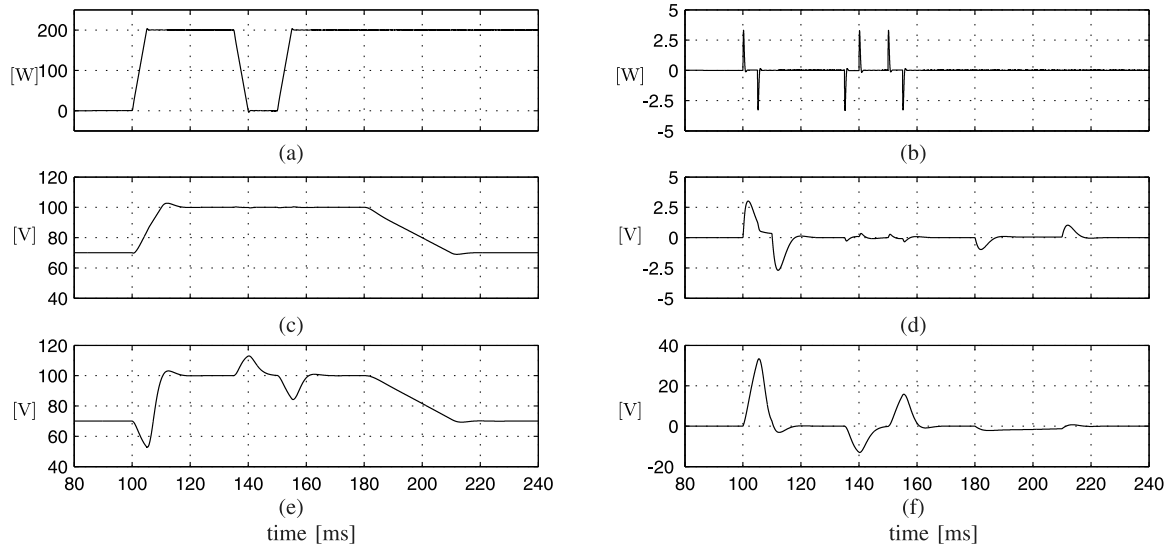

Fig. 4. Simulation results to a load power change. (a) Estimated load power $\hat{P}_o$. (b) Error signal $P_o - \hat{P}_o$. (c) Voltage v_c in the output capacitor for proposed controller. (d) Error signal $v_c^* - v_c$. (e) Voltage v_c in the output capacitor for linear controller. (f) Error signal $v_c^* - v_c$.

This yield

$$||e(t)|| \leq exp^{-\gamma_1 t}||e(0)|| + \frac{\gamma_2}{\gamma_1}(1 - exp^{-\gamma_1 t}) \qquad (48)$$

which shows that the observer error is bounded in presence of parameter uncertainties.

B. Full System Stability

In this section, the effect of a mismatch in parameters $\hat{L}$ and $\hat{C}$ on the stability of the closed-loop controller will be analyzed. The autonomous closed-loop system is linearized at an operation point in the appendix, and the resulting system matrix A_l is defined in (62). The variables that can change in this matrix are $v_{c0}, P_{o0}, \hat{L}$, and $\hat{C}$ (the initial inductor current is $i_{l0} = P_{o0}/v_{c0}$), where the subscript 0 indicates evaluated at the operation point. For each set of parameters, the eigenvalues of A_l are found, and the real part of these which is closest to zero (instability) is plotted. Fig. 3 shows this plot, for $v_{c0} = 100$ V, $0 \leq P_{o0} \leq 500$ W, $0.8\ L \leq \hat{L} \leq 1.2\ L$, and $0.35\ C \leq \hat{C} \leq 1.2\ C$. As can be seen, all the eigenvalues remain in the negative semiplane, which shows that the system is closed-loop stable even to the proposed parameter mismatches.

V. Simulation Results

The system was simulated with $L = 2.98$ mH, $C = 99.52\ \mu$F, and $E = 200$ V. Both load power and voltage reference changes were simulated. The load power was changed from 0 to 200 W and *vice versa* in 5 ms with a ramp profile. The voltage reference was changed from 65 to 100 V first in 10 ms and then from 100 to 65 V in 30 ms, both with a ramp profile. For the controller, a settling time $t_{\rm set} = 10$ ms was chosen. According to (17)–(19), the gains to achieve this $t_{\rm set}$ are: $K_1 = 3.37 \times 10^6$, $K_2 = 4.7 \times 10^3$, and $K_3 = 1.22 \times 10^9$. For the observer, a settling time $t_{\rm seto} = 1$ ms was chosen. According to (27)–(29), the gains to achieve this $t_{\rm seto}$ are: $g_1 = 7.82 \times 10^3$ and $g_2 = 3.12 \times 10^7$. The output voltage reference was chosen $v_c^* = 100$ V.

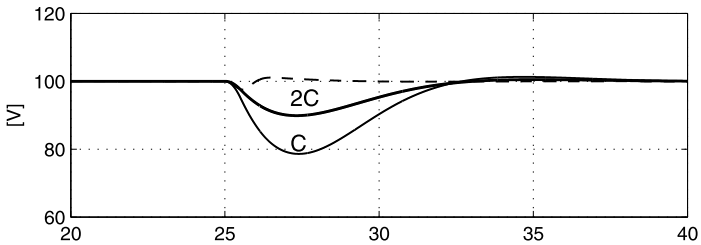

Fig. 5. Transient response of the linear controller to a load disturbance for output capacitor of value C and 2C (solid line) along with the response of the proposed controller for output capacitor of value C (dashed line).

The proposed controller was compared against a linear controller. The linear controller used here for comparison is a full state feedback with an integral action. This controller is implemented as

$$d = -k_1 i_l - k_2 v_c - k_3 x_{\rm int} \qquad (49)$$

where $k_1 = 0.073$, $k_2 = 0.00145$, and $k_3 = 1.809$ are the feedback gains, and $x_{\rm int}$ is the additional state corresponding to the integral action. The controller is tuned using the linearization of the systems (1) and (2), evaluated at the chosen point of operation (see appendix, Section E). For comparison purposes, the gains are chosen placing the closed-loop poles at the same locations as in the proposed controller, through (17)–(19) and Ackerman's method.

Fig. 4(a) shows the estimated power $\hat{P}_o$ and Fig. 4(b) shows the error between the actual power P_o and $\hat{P}_o$. This last figure shows that the maximum power estimation error is 1.6% of the maximum power. As can be seen, the proposed observer is able to track the power changes after a short transient. Fig. 4(c) shows the capacitor voltage v_c for the proposed controller, and Fig. 4(d) shows the error between the reference voltage and

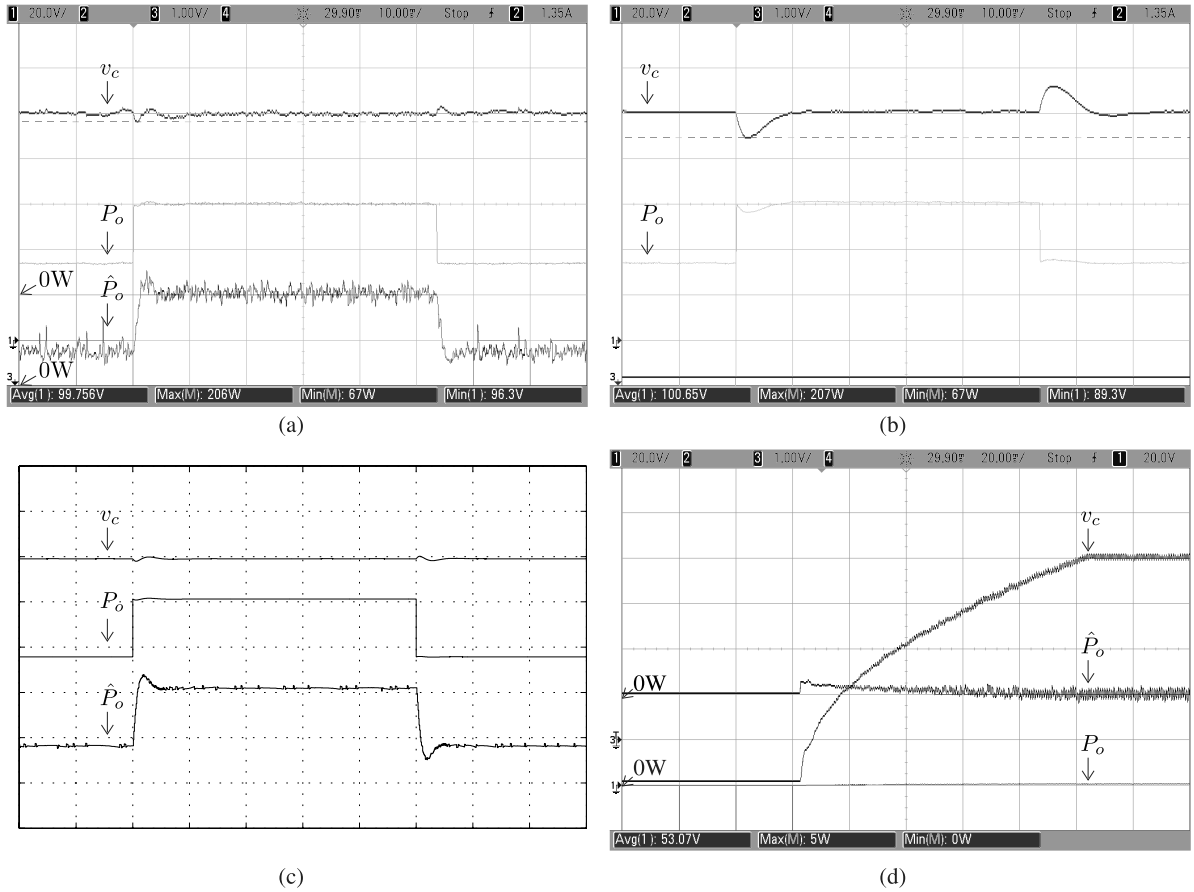

Fig. 6. Experimental results to load power step from 67 to 206 W. CH1: v_c, CH2: load current (not shown), MATH: P_o (CH1$\times$ CH2), CH3: $\hat{P}_o$. Scales: time 10 ms/div, v_c 20 V/div, $P_o/\hat{P}_o$ 100 W/div. (a) Proposed controller. (b) Linear controller. (c) Simulation results proposed controller. (d) Zero power startup.

the capacitor voltage. This last figure shows that the maximum voltage tracking error is 3% of the 100 V. As can be seen, the transients during simultaneous voltage reference and load power changes are small. Also, the transients during load power changes alone are even smaller, and converge within 1 ms, as determined by the observer convergence time. Finally, Fig. 4(e) shows the capacitor voltage v_c for the linear controller, and Fig. 4(f) shows the error between the voltage reference and the capacitor voltage. This last figure shows that the maximum voltage tracking error is 33% of the 100 V. As can be seen, the linear controller has very large transients during simultaneous voltage and load power changes. Note also that when only the load power changes, there are also large transients.

For this plant-controller system, it is possible to improve the disturbance rejection capabilities by increasing the output capacitor value. Fig. 5 compares the transient response of v_c to a load change from 0 to 200 W in 5 ms when the value of the output capacitor is C and 2C. This figure shows that increasing the capacitor value clearly improves the transient response. However, a larger capacitor increases the cost of the system, and even twice as much capacitance cannot match the transient performance improvement achieved with the proposed controller, which is also shown in dashed line in the figure for an output capacitor of value C. Simulation results shows that in order to achieve a dynamic response similar to that of the proposed controller, the capacitance must be increased to approximately 20C.

These simulation results show that the proposed observer clearly improves the transient performance of the controller, and it does so without increasing the cost of the system. This is a desirable feature, which is achieved thanks to the feedforward compensation.

VI. Experimental Results

For the experimental results, the converter was implemented using IGBTs IRG4PH50UD, with $L = 2.98$ mH and $C = 99.52\,\mu$F. The parasitic resistance of the inductance was 340 mΩ, and the series resistance of the capacitor was 480 mΩ. The controller was implemented in a fixed point digital signal processor (DSP) TMS320F2812 working with a clock frequency of 150 MHz. The sampling time used for the discrete implementation of the controller was $T_s = 50\,\mu$s, and the pulse width modulator frequency was set to 20 kHz. The discretization of the controller was performed integrating the differential equations through the forward Euler integrator. The measured signals v_c and i_l were filtered using an *RC* antialias filter with a cut-off frequency of 2340 Hz. A power dc voltage source set to $E = 200$ V was used as an input source, and a controlled current source was used as a load. The load was implemented using an

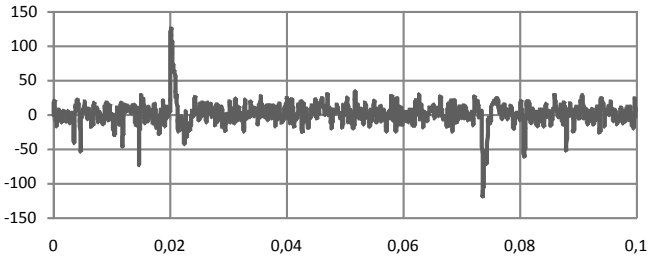

Fig. 7. Power estimation error [W].

SLH-500-6-1800 AC/DC electronic load. This load cannot be configured to behave as a constant power load, but it can be configured to behave as a constant current load. Even though this type of load was not modeled, the experimental results will show that the proposed strategy is still capable of improving the transient performance to load disturbances. Due to the limitations of the load, which only allows to specify a current step through crest factor, the results were obtained when power step from 67 to 207 W is performed.

For the controller, the gains were the same as in the previous simulations and for the observer, the gains were obtained from $t_{\text{seto}} = 4$ ms, which result $g_1 = 1.95e3$ and $g_2 = 1.95e6$. Fig. 6 shows the experimental results obtained for the proposed controller and the linear controller.

Fig. 6(a) shows the experimental results for the proposed controller. Here, the capacitor voltage v_c, the actual power P_o, and the estimated power $\hat{P}_o$ are shown. In channel 1, the capacitor voltage was captured; in channel 2 (not shown), the output current; and in channel 3, the estimated power. In order to capture the estimated power, this signal was sent to a PWM output of the DSP, which was then filtered through an *RC* filter with cutoff frequency of 2340 Hz. In order to obtain the instantaneous output power, the product between the capacitor voltage measurement and the output current measurement was performed with the oscilloscope. As can be seen, the capacitor voltage presents a small transient during the power step. This voltage converges to steady state in 5 ms. This transient matches that of the estimated power. Fig. 7 shows the power estimation error obtained from the data of MATH and CH3 of Fig. 6(a). As the figure shows, the power error is larger than that of the simulation results. This is due to the load step being a current step instead of a power step. However, the figure shows that the estimated power tracks the actual power within the expected time.

For comparison, Fig. 6(b) shows the experimental results for the linear controller. The signals shown are the capacitor voltage v_c and the actual power P_o. As can be seen, the overshoot of v_c during the power transient is significantly larger than that observed with the proposed controller. This performance is similar to the performance obtained with the controller proposed in [18]. On the other hand, the steady-state voltage ripple of the linear controller seems smaller than that of the proposed controller. This is because the proposed controller has a larger equivalent bandwidth than the linear controller. For this reason, there is a little more ripple in steady state. The value of this ripple depends on the gain of the observer. Therefore, there is a tradeoff between convergence speed and steady-state ripple.

The comparison of both figures shows that the proposal improves the transient performance. This feature is achieved because a disturbance sensorless feedforward compensation has been included. Since it is a sensorless compensation, the designed controller is cheaper and rugged.

To verify the validity of the experimental results to the type of load used (constant current load), the experimental setup was replicated in simulation. Fig. 6(c) shows the simulation results of the proposed controller under the same conditions as the experimental setup. As can be seen, the system behaves as expected.

In Fig. 6(d), the behavior of the system during the start up of the converter is shown. To diminish the inductor L current peak, the output voltage reference v_c^* was taken from 0 to 100 V in 100 ms through a ramp. As can be seen in the figure, the controller is capable of maintaining the output at the reference voltage value even at zero load power.

VII. Conclusion

A controller for buck converters feeding constant power loads has been presented. The proposed controller combines a nonlinear feedback law with a feedforward one. This combination allows us to obtain a very fast dynamical response to sudden power load variations. A theoretical frame which supports the proposed algorithm as well as a methodology to choose its parameters has been given. To validate the proposal, simulation and experimental results have been presented. From these results, it can be concluded that the proposed controller allows to reduce the output voltage transient time during load transients, when compared to a linear controller if an output capacitor of the same value is used in both controllers.

Appendix

A. Plant Linearization: Replacing (8) into (6) and applying Taylor's first-order linearization to the resulting equation and to (5), it results

$$\triangle \dot{z}_1 = \triangle z_2 \tag{50}$$

$$\triangle \dot{z}_2 = \left.\frac{d\dot{z}_2}{d\hat{m}}\right|_0 \triangle \hat{m} + \left.\frac{d\dot{z}_2}{dv_c}\right|_0 \triangle v_c + \left.\frac{d\dot{z}_2}{di_l}\right|_0 \triangle i_l + \left.\frac{d\dot{z}_2}{d\hat{P}_o}\right|_0 \triangle \hat{P}_o + \left.\frac{d\dot{z}_2}{dd_1}\right|_0 \triangle d_1 \tag{51}$$

where $\left.\frac{d\dot{z}_2}{d\hat{m}}\right|_0 = \left.\frac{d\dot{z}_2}{dd_1}\right|_0 = \frac{\hat{L}}{L}$; $\left.\frac{d\dot{z}_2}{dv_c}\right|_0 = \rho\frac{P_{o0}\, i_{l0}}{v_{c0}^2}$; $\left.\frac{d\dot{z}_2}{di_l}\right|_0 = \left(2i_{l0} - \frac{P_{o0}}{v_{c0}}\right)\rho$; $\left.\frac{d\dot{z}_2}{d\hat{P}_o}\right|_0 = \left(\frac{1}{C} - \rho\right)\frac{i_{l0}}{v_{c0}}$; $\rho = \frac{1}{C} - \frac{\hat{L}}{\hat{C}L}$ and the subscript 0 indicates evaluated at the operation point. Linearizing (3) and (4), we obtain

$$\triangle z_1 = C v_{c0} \triangle v_c \tag{52}$$

$$\triangle z_2 = i_{l0} \triangle v_c + v_{c0} \triangle i_l. \tag{53}$$

Then, applying these equations in (51), it results:

$$A_l = \begin{bmatrix} 0 & 1 & 0 & 0 & 0 \\ G_{z_1} - [(g_1 G_{\hat{P}_o} + g_2 G_{\hat{m}}) & & & & \\ +G_{d_1}(K_1 + K_2 g_1)]\frac{\hat{C}}{C} & G_{z_2} - G_{d_1} K_2 & -G_{d_1} K_3 & G_{\hat{P}_o} - G_{d_1} K_2 & G_{\hat{m}} \\ (g_1^2 - g_2)\frac{\hat{C}}{C} & g_1 & 0 & -g_1 & 1 \\ g_1 g_2 \frac{\hat{C}}{C} & g_2 & 0 & -g_1 & 0 \end{bmatrix}. \quad (62)$$

$$\triangle \dot{z}_2 = G_{\hat{m}} \triangle \hat{m} + G_{z_1} \triangle z_1 + G_{z_2} \triangle z_2 + G_{\hat{P}_o} \triangle \hat{P}_o + G_{d_1} \triangle d_1 \quad (54)$$

where $G_{\hat{m}} = G_{d_1} = \frac{d\dot{z}_2}{d\hat{m}}\big|_0$; $G_{z_2} = \frac{1}{v_{c0}} \frac{d\dot{z}_2}{di_l}\Big|_0$; $G_{z_1} = \frac{1}{C v_{c0}} \left(\frac{d\dot{z}_2}{dv_c}\Big|_0 - i_{l0} G_{z_2} \right)$ y $G_{\hat{P}_o} = \frac{d\dot{z}_2}{d\hat{P}_o}\Big|_0$.

B. Observer Linearization: Linearizing (9), it results

$$\triangle \tilde{z}_1 = \frac{\hat{C}}{C} \triangle z_1 \quad (55)$$

then, applying this equation to the linearization of the observer (32)–(35), it results

$$\triangle \dot{\varepsilon}_1 = (g_1^2 - g_2)\frac{\hat{C}}{C} \triangle z_1 + g_1 \triangle z_2 - g_1 \triangle \varepsilon_1 + \triangle \varepsilon_2 \quad (56)$$

$$\triangle \dot{\varepsilon}_2 = g_1 g_2 \frac{\hat{C}}{C} \triangle z_1 + g_2 \triangle z_2 - g_2 \triangle \varepsilon_1 \quad (57)$$

$$\triangle \hat{P}_o = \triangle \varepsilon_1 - g_1 \frac{\hat{C}}{C} \triangle z_1 \quad (58)$$

$$\triangle \hat{m} = \triangle \varepsilon_2 - g_2 \frac{\hat{C}}{C} \triangle z_1. \quad (59)$$

C. Controller Linearization: The linearization of the controller (14) results

$$\triangle d_1 = -(K_1 + K_2 g_1)\frac{\hat{C}}{C} \triangle z_1 - K_2 \triangle z_2 + K_2 \triangle \varepsilon_1 - K_3 \triangle z_3 \quad (60)$$

where

$$\triangle \dot{z}_3 = \frac{\hat{C}}{C} \triangle z_1. \quad (61)$$

D. System Matrix: From (54)–(61), defining the state vector as $\triangle \vec{z} = [\triangle z_1 \ \triangle z_2 \ \triangle z_3 \ \triangle \varepsilon_1 \ \triangle \varepsilon_2]^T$, the system matrix of the linearized autonomous system results (62) as shown top of the page

E. Linear Full State Feedback Controller Tuning: The linearization is obtained deriving (1) with respect to d and v_c, and (2) with respect to i_l and v_c. The state variable description of the resulting linearized system is

$$\begin{bmatrix} \triangle \dot{i}_l \\ \triangle \dot{v}_c \\ \dot{x}_{int} \end{bmatrix} = \underbrace{\begin{bmatrix} 0 & -\frac{1}{L} & 0 \\ \frac{1}{C} & \frac{P_{o0}}{C v_{c0}^2} & 0 \\ 0 & 1 & 0 \end{bmatrix}}_{A_l} \begin{bmatrix} \triangle i_l \\ \triangle v_c \\ x_{int} \end{bmatrix} + \underbrace{\begin{bmatrix} \frac{E}{L} \\ 0 \\ 0 \end{bmatrix}}_{B_l} \triangle d \quad (63)$$

where $\triangle$ denotes a linearized variable, and P_{o0} and v_{c0} are the load power and capacitor voltage at the point of operation. With the state matrix and vector A_l and B_l, the feedback gains can be chosen through any pole placement method, such as Ackerman's method.

REFERENCES

[1] Directorate general for research sustainable energy systems, "European technology platform smartgrids vision and strategy for Europe's electricity networks of the future," *RTD Info*, 2006.

[2] D. Boroyevich, I. Cvetkovic, R. Burgos, and D. Dong, "Intergrid: A future electronic energy network?" *IEEE J. Emerging Sel. Topics Power Electron.*, vol. 1, no. 3, pp. 127–138, Sep. 2013.

[3] M. Pahlevaninezhad, D. Hamza, and P. Jain, "An improved layout strategy for common-mode EMI suppression applicable to high-frequency planar transformers in high-power dc/dc converters used for electric vehicles," *IEEE Trans. Power Electron.*, vol. 29, no. 3, pp. 1211–1228, Mar. 2014.

[4] M. Yilmaz and P. Krein, "Review of the impact of vehicle-to-grid technologies on distribution systems and utilities interfaces," *IEEE Trans. Power Electron.*, vol. 28, no. 12, pp. 5673–5689, Dec. 2013.

[5] R. Silva-Ortigoza, V. Hernandez-Guzman, M. Antonio-Cruz, and D. Munoz-Carrillo, "DC/DC buck power converter as a smooth starter for a dc motor based on a hierarchical control," *IEEE Trans. Power Electron.*, vol. 30, no. 2, pp. 1076–1084, Feb. 2015.

[6] J. Sebastian, P. Fernandez-Miaja, F. Ortega-Gonzalez, M. Patino, and M. Rodriguez, "Design of a two-phase buck converter with fourth-order output filter for envelope amplifiers of limited bandwidth," *IEEE Trans. Power Electron.*, vol. 29, no. 11, pp. 5933–5948, Nov. 2014.

[7] M. Rodriguez, Y. Zhang, and D. Maksimovic, "High-frequency PWM buck converters using gan-on-sic hemts," *IEEE Trans. Power Electron.*, vol. 29, no. 5, pp. 2462–2473, May 2014.

[8] M. Truntic and M. Milanovic, "Voltage and current-mode control for a buck-converter based on measured integral values of voltage and current implemented in FPGA," *IEEE Trans. Power Electron.*, vol. 29, no. 12, pp. 6686–6699, Dec. 2014.

[9] C. Zhang, J. Wang, S. Li, B. Wu, and C. Qian, "Robust control for PWM-based dc-dc buck power converters with uncertainty via sampled-data output feedback," *IEEE Trans. Power Electron.*, vol. 30, no. 1, pp. 504–515, Jan. 2015.

[10] C. Chia, C.-H. Chang, P.-S. Lei, and H.-M. Chen, "A two-phase fully-integrated dc-dc converter with self-adaptive DCM control and GIPD passive components," *IEEE Trans. Power Electron.*, vol. 30, no. 6, pp. 3252–3261, Jun. 2014.

[11] P. Cheng, M. Vasic, O. Garcia, J. Oliver, P. Alou, and J. Cobos, "Minimum time control for multiphase buck converter: Analysis and application," *IEEE Trans. Power Electron.*, vol. 29, no. 2, pp. 958–967, Feb. 2014.

[12] S. C. Smithson and S. S. Williamson, "Constant power loads in more electric vehicles-an overview," in *Proc. IEEE 38th Annu. Conf. Ind. Electron. Soc.*, 2012, pp. 2914–2922.

[13] A. M. Rahimi and A. Emadi, "An analytical investigation of dc/dc power electronic converters with constant power loads in vehicular power systems," *IEEE Trans. Veh. Technol.*, vol. 58, no. 6, pp. 2689–2702, Jul. 2009.

[14] C. H. Rivetta, A. Emadi, G. A. Williamson, R. Jayabalan, and B. Fahimi, "Analysis and control of a buck dc-dc converter operating with constant power load in sea and undersea vehicles," *IEEE Trans. Ind. Appl.*, vol. 42, no. 2, pp. 559–572, Mar./Apr. 2006.

[15] E. A. Kai Strunz and D. N. Huu, "DC microgrid for wind and solar power integration," *IEEE J. Emerging Sel. Topics Power Electron.*, vol. 2, no. 1, pp. 115–126, Mar. 2014.
[16] A. Kwasinski and C. N. Onwuchekwa, "Dynamic behavior and stabilization of dc microgrids with instantaneous constant-power loads," *IEEE Trans. Power Electron.*, vol. 26, no. 3, pp. 822–834, Mar. 2011.
[17] D. J. Becker and B. Sonnenberg, "DC microgrids in buildings and data centers," in *Proc IEEE 33rd Int. Telecommun. Energy Conf.*, 2011, pp. 1–7.
[18] J. Wang and D. Howe, "A power shaping stabilizing control strategy for dc power systems with constant power loads," *IEEE Trans. Power Electron.*, vol. 23, no. 6, pp. 2982–2989, Nov. 2008.
[19] A. Emadi, A. Khaligh, C. H. Rivetta, and G. A. Williamson, "Constant power loads and negative impedance instability in automotive systems: Definition, modeling, stability, and control of power electronic converters and motor drives," *IEEE Trans. Veh. Technol.*, vol. 55, no. 4, pp. 1112–1125, Jul. 2006.
[20] M. Cespedes, L. Xing, and J. Sun, "Constant-power load system stabilization by passive damping," *IEEE Trans. Power Electron.*, vol. 26, no. 7, pp. 1832–1836, Jul. 2011.
[21] J. G. Ciezki and R. W. Ashton, "The design of stabilizing controls for shipboard dc-to-dc buck choppers using feedback linearization techniques," in *Proc. IEEE 29th Annu. Power Electron. Spec. Conf.*, 1998, pp. 335–341.
[22] J. Zeng, Z. Zhang, and W. Qiao, "An interconnection and damping assignment passivity-based controller for a dc-dc boost converter with a constant power load," *IEEE Trans. Ind. Appl.*, vol. 50, no. 4, pp. 2314–2322, Jul./Aug. 2014.
[23] Y. Zhao, W. Qiao, and D. Ha, "A sliding-mode duty-ratio controller for dc/dc buck converters with constant power loads," *IEEE Trans. Ind. Appl.*, vol. 50, no. 2, pp. 1448–1458, Mar./Apr. 2014.
[24] A. P. N. Tahim, D. J. Pagano, and E. Ponce, "Nonlinear control of dc-dc bidirectional converters in stand-alone dc microgrids," in *Proc. IEEE 51st Conf. Decision Control*, Maui, HI, USA, Dec. 2012, pp. 3068–3073.
[25] H. Kakigano, Y. Miura, and T. Ise, "Distribution voltage control for dc microgrids using fuzzy control and gain-scheduling technique," *IEEE Trans. Power Electron.*, vol. 28, no. 5, pp. 2246–2258, May 2013.
[26] A. M. Rahimi and A. Emadi, "Active damping in dc/dc power electronic converters: A novel method to overcome the problems of constant power loads," *IEEE Trans. Ind. Electron.*, vol. 56, no. 5, pp. 1428–1439, May 2009.
[27] A. Gensior, O. Woywode, J. Rudolph, and Guldner,"On differential flatness, trajectory planning, observers, and stabilization for dc-dc converters," *IEEE Trans. Circuits Syst. I, Reg. Papers*, vol. 53, no. 9, pp. 2000–2010, Sep. 2006.
[28] Y. Li, K. R. Vannorsdel, A. J. Zirger, M. Norris, and D. Maksimovic, "Current mode control for boost converters with constant power loads," *IEEE Trans. Circuits Syst. I, Reg. Papers*, vol. 59, no. 1, pp. 198–206, Jan. 2012.
[29] A. E. León, J. A. Solsona, C. Busada, H. Chiacchiarini, and M. I. Valla, "High-performance control of a three-phase voltage-source converter including feedforward compensation of the estimated load current," *Energy Convers. Manag.*, vol. 50, pp. 2000–2008, Aug. 2009.
[30] A. E. León, J. A. Solsona, and M. I. Valla, "Exponentially convergent estimator to improve performance of voltage source converters," *IET Power Electron.*, vol. 3, no. 5, pp. 668–680, Sep. 2010.
[31] B.-W. Lai and C. S. Sims, "Disturbance rejection and tracking using output feedforward control," *IEEE Trans. Automat. Control*, vol. 35, no. 6, pp. 749–752, Jun. 1990.
[32] H. K. Khalil, *Nonlinear Systems*, 3rd ed. Englewood Cliffs, NJ, USA: Prentice-Hall, 2002.
[33] G. F. Franklin, J. D. Powell, and A. Emami-Naeini, *Feedback Control of Dynamic Systems.* Reading, MA, USA: Addison-Wesley, 1993.

Jorge A. Solsona (SM'04) received the Electronics Engineering and Doctorate degrees from the Universidad Nacional de La Plata, La Plata, Argentina, in 1986 and 1995, respectively.

He is currently with the Departamento de Ingeniería Eléctrica y de Computadoras, Instituto de Investigaciones en Ingeniería Eléctrica "Alfredo C. Desages," Universidad Nacional del Sur, Bahía Blanca, Argentina, where he is a Professor, and also with CONICET. He is involved in teaching and research on control theory and its applications to electromechanical systems.

Sebastián Gómez Jorge received the Electronics Engineering, M.S., and Doctorate degrees from the Universidad Nacional del Sur, Bahía Blanca, Argentina, in 2006, 2009, and 2011, respectively.

He is currently with the Departamento de Ingeniería Eléctrica y de Computadoras, Instituto de Investigaciones en Ingeniería Eléctrica "Alfredo C. Desages," Universidad Nacional del Sur, Bahía Blanca, Argentina, where he is a Graduate Teaching Assistant, and also with CONICET.

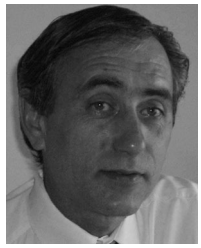

Claudio A. Busada was born in Bahía Blanca, Argentina, on March 13, 1962. He received the Electrical Engineering degree and the Doctorate degree in control systems both from the Universidad Nacional del Sur, Bahía Blanca, in 1989 and 2004, respectively.

From 1988 to 2004, he was with the Mechanic and Electrical Department, City of Bahía Blanca. Since 1989, he has been with the Departamento de Ingeniería Eléctrica y de Computadoras, Universidad Nacional del Sur, where he is a Professor. He is also a Researcher of the Instituto de Investigaciones en Ingeniería Eléctrica "Alfredo C. Desages." His research interests include power electronics, rotating machinery, active filters, automatic control, and integration of distributed energy systems.